



# Multi-frequency electrical impedance tomography as a non-invasive tool to characterize and monitor crop root systems

Maximilian Weigand and Andreas Kemna

Department of Geophysics, University of Bonn, Meckenheimer Allee 176, 53115 Bonn, Germany

*Correspondence to:* Maximilian Weigand (mweigand@geo.uni-bonn.de)

Received: 23 April 2016 – Discussion started: 23 August 2016

Revised: 27 January 2017 – Accepted: 28 January 2017 – Published: 28 February 2017

**Abstract.** A better understanding of root–soil interactions and associated processes is essential in achieving progress in crop breeding and management, prompting the need for high-resolution and non-destructive characterization methods. To date, such methods are still lacking or restricted by technical constraints, in particular the characterization and monitoring of root growth and function in the field. A promising technique in this respect is electrical impedance tomography (EIT), which utilizes low-frequency ( $< 1 \text{ kHz}$ )-electrical conduction- and polarization properties in an imaging framework. It is well established that cells and cell clusters exhibit an electrical polarization response in alternating electric-current fields due to electrical double layers which form at cell membranes. This double layer is directly related to the electrical surface properties of the membrane, which in turn are influenced by nutrient dynamics (fluxes and concentrations on both sides of the membranes). Therefore, it can be assumed that the electrical polarization properties of roots are inherently related to ion uptake and translocation processes in the root systems. We hereby propose broadband (mHz to hundreds of Hz) multi-frequency EIT as a non-invasive methodological approach for the monitoring and physiological, i.e., functional, characterization of crop root systems. The approach combines the spatial-resolution capability of an imaging method with the diagnostic potential of electrical-impedance spectroscopy. The capability of multi-frequency EIT to characterize and monitor crop root systems was investigated in a rhizotron laboratory experiment, in which the root system of oilseed plants was monitored in a water-filled rhizotron, that is, in a nutrient-deprived environment. We found a low-frequency polarization response of the root system, which enabled the successful delineation of its spatial extension. The magnitude of the overall polarization re-

sponse decreased along with the physiological decay of the root system due to the stress situation. Spectral polarization parameters, as derived from a pixel-based Debye decomposition analysis of the multi-frequency imaging results, reveal systematic changes in the spatial and spectral electrical response of the root system. In particular, quantified mean relaxation times (of the order of 10 ms) indicate changes in the length scales on which the polarization processes took place in the root system, as a response to the prolonged induced stress situation. Our results demonstrate that broadband EIT is a capable, non-invasive method to image root system extension as well as to monitor changes associated with the root physiological processes. Given its applicability on both laboratory and field scales, our results suggest an enormous potential of the method for the structural and functional imaging of root systems for various applications. This particularly holds for the field scale, where corresponding methods are highly desired but to date are lacking.

## 1 Introduction

Interest in and development of non-invasive methods for the structural and functional characterization as well as the monitoring of root systems and the surrounding rhizosphere have substantially increased in recent years (e.g., Heřmanšká et al., 2015, and references therein). This trend is driven mostly by the need to improve crop management and breeding techniques, and to reduce fertilizer usage (e.g., Heege, 2013). In this context, various non-invasive methods for the investigation and characterization of crop root systems have been proposed (for a comprehensive overview of current methods, both for laboratory and field studies, see Mancuso,

2012). These methods include light transmission tomography (e.g., Pierret et al., 2003), X-ray computer tomography (e.g., Gregory et al., 2003; Pierret et al., 2003), neutron radiography (e.g., Willatt et al., 1978), magnetic resonance imaging (e.g., Metzner et al., 2015, and references therein), electrical resistivity tomography (ERT) (e.g., Mancuso, 2012), electrical capacitance measurements, and electrical impedance spectroscopy (EIS) (see Mancuso, 2012; Anderson and Hopmans, 2013, and references therein). However, most of these methods cannot, or only under special circumstances, be used at the field scale, or they lack sensitivity to structural or physiological features of the rhizosphere (e.g., Mancuso, 2012).

Electrical methods, including both tomographic and spectroscopic approaches, are gaining importance for root research due to their universal applicability at different scales and the recognized potential to provide pertinent information on root systems via their electrical properties. Advances in measurement accuracy (Zimmermann et al., 2008) and large-scale deployments (e.g., Johnson et al., 2012; Loke et al., 2013) allow imaging studies with high spatial and temporal resolution at both laboratory and field scales (see, e.g., Kemna et al., 2012; Singha et al., 2014).

Electrical resistance measurements on root systems have been related to root age (Anderson and Higinbotham, 1976), to absorbing root surfaces of trees (Aubrecht et al., 2006; Čermák et al., 2006), and to surface area in contact with the ambient solution (Cao et al., 2010). The measured resistances are usually interpreted by means of equivalent electrical circuit models of the root–soil continuum, and relations to biological properties are analyzed in terms of the circuit model parameters. Electrical imaging applications on crop root systems, however, are relatively rare. ERT has been used to map root zones (al Hagrey, 2007; Amato et al., 2008, 2009; al Hagrey and Petersen, 2011; Rossi et al., 2011) and to monitor water content in maize fields (Sayeddin and Doussan, 2009; Beff et al., 2013) and under an apple orchard (Boaga et al., 2013). Whalley et al. (2017) showed that ERT can be used in the field to indirectly phenotype root systems by monitoring water content distributions over time.

As pointed out by Urban et al. (2011), resistance methods for root characterization suffer from an inherent ambiguity of effective conductivity (or resistivity), making interpretation difficult. Polarization properties, on the other hand, provide valuable additional information, in particular if their spectral variation is explored. In geophysics, corresponding measurement approaches are referred to as induced polarization (IP) or spectral induced polarization (SIP) methods, since the polarization is provoked by an impressed electric field. A wide range of studies have investigated electrical polarization properties of plant root systems, mostly in terms of capacitances, using alternating-current measurements at a particular frequency (e.g., Walker, 1965; Chloupek, 1972; Dvořák et al., 1981; Dalton, 1995; Aulen and Shipley, 2012; Dietrich et al., 2013). Correlations of varying strength have been found between measured capacitances and root (dry)

mass, root surface, and various attributes associated with physiological processes such as root development. For example, Ellis et al. (2013) used an improved measurement setup to investigate the relation of electrical capacitances to root mass, root surface area, and root length in soil experiments. For an overview of studies using electrical capacitance measurements on root systems, we refer the reader to Kormanek et al. (2015). While in the above-mentioned studies single-frequency capacitance measurements were used, more recent studies also focused on the analysis of spectral measurements covering a broad frequency range, in terms of both capacitances (Ozier-Lafontaine and Bajazet, 2005) and impedances (Ozier-Lafontaine and Bajazet, 2005; Cao et al., 2011; Zanetti et al., 2011; Cseresnyés et al., 2013; Repo et al., 2014).

Research has also been conducted on electrical properties at the cellular scale, including electrical surface properties of cell membranes, also called plasma membranes (e.g., Kinraide, 1994; Wang et al., 2011). An electrical double layer (EDL) forms at an electrically charged surface in contact with an electrolyte (e.g., Lyklema, 2005). This EDL gives rise to electrical polarizability (e.g., Lyklema et al., 1983), which can be measured with EIS or electrical impedance tomography (EIT). Accordingly, variations in the EDL characteristics related to structural or functional changes in the root system should manifest in electrical impedance measurements. According to Kinraide et al. (1998) cell walls can be assumed to be near ionic equilibrium with the surrounding electrolyte and thus do not contribute to the formation of EDLs in biomaterial.

Imaging of IP or SIP parameters has, so far, to our knowledge, not been applied to the field of root research. However, various applications in near-surface petro- and biogeophysics have been successful. For example, spectral (i.e., multi-frequency) EIT was used to map subsurface hydrocarbon contamination at an industrial site (Flores Orozco et al., 2012a) and to monitor uranium precipitation induced by bacterial injections within the frame of contaminated site remediation (Flores Orozco et al., 2013) – both studies demonstrating the field-scale applicability of the method for subsurface (bio)geochemical characterization. Martin and Günther (2013) applied EIT to investigate fungus infestation of trees; however, in the imaging they did not take the spectral variation into account.

In the present work, we propose broadband (mHz – kHz) multi-frequency EIT as an imaging tool for the physiological, i.e., functional, characterization of crop root systems. This novel approach for functional root imaging combines the spatial resolution benefits of EIT with the diagnostic capability of EIS, and builds upon instrumentation and processing tools that have been developed in recent years. Analogous to the now widely accepted interpretation of SIP signatures of soils and rocks in terms of textural and mineral surface characteristics, we hypothesize that the SIP response of crop root systems, which is imaged with the proposed methodology, is

directly related to physicochemical processes in the vicinity of electrical double layers forming in association with root physiological activity (e.g., nutrient uptake) at specific scales of the root system.

Besides the spatial delineation and monitoring of active root zones in terms of polarization magnitude, we aim at the analysis of the imaged SIP response in terms of relaxation times, which provides information on the spatial length scale at which the underlying processes occur. Relaxation times are determined using the Debye decomposition scheme, a phenomenological model that can describe a wide variety of SIP signatures (e.g., Nordsiek and Weller, 2008; Weigand and Kemna, 2016). A similar procedure to analyse SIP signatures is also proposed by Ozier-Lafontaine and Bajazet (2005) for the analysis of SIP signatures measured on root systems.

To demonstrate the proposed methodology, we conducted a laboratory experiment on oilseed plants grown in hydroponic conditions. The plants were placed in a rhizotron container filled with tap water and monitored using multi-frequency EIT in the course of prolonged nutrient deficiency. The recovered spectral electrical signatures at various time steps were analyzed with regard to total polarization strength and dominant relaxation timescales, and qualitatively related to the macroscopic reaction of the root system to the induced stress situation.

The next section shortly reviews electrical measurements on, and the underlying polarization properties of root systems. Then, the geophysical methods used in the presented study are described, followed by the experimental setup and data acquisition/processing steps. The last two sections present the results and discuss methodological and biological aspects of the experiment.

## 2 Electrical properties and measurements of root systems

This section develops our working hypotheses regarding the electrical polarization of crop root systems. A more detailed description of the EDL is given and linked to the measurement methodology. Moreover, we shortly review previous works on the small-scale (cells and cell suspensions) polarization of biomatter and the approaches used to analyze polarization measurements on whole root systems.

### 2.1 Electrical double layer polarization

Electrical conduction properties of soils are primarily determined by electrolytic soil water conductivity, i.e., ion concentration and mobility, and the interface conduction processes at water–mineral interfaces. Electrical polarization properties originate mainly in ion accumulation processes in constrictions of the pore network and at water–mineral interfaces. If surfaces are electrically charged and in contact with

an electrolyte such as those found at mineral grain surfaces or cell membranes, electrical double layers (EDLs) form, which comprise the so-called Stern layer of bound counterions and the so-called diffusive layer. The latter forms in the equilibrium of electromigrative and diffusive ion fluxes, and is characterized by ion concentration gradients. The EDL is affected by external electric fields, manifesting an induced polarization (IP), and takes a finite time (relaxation time) to reach equilibrium again once an impressed external field is turned off (e.g., Lyklema, 2005). Models of both Stern layer polarization (the build-up of counterion concentration gradients in the Stern layer in the direction of the external electric field) (e.g., Schwarz, 1962; Leroy et al., 2008) and diffuse layer polarization (the build-up of counterion and coion concentration gradients in the diffuse layer in the direction of the external electric field) (e.g., Dukhin and Shilov, 1974; Fixman, 1980) have been developed, as well as models encompassing both the Stern layer and the diffuse layer (e.g., Lyklema et al., 1983; Razilov and Dukhin, 1995). In a porous system such as soil, diffuse layer polarization is also referred to as membrane polarization since the resultant ion concentration gradients, for instance along a pore constriction, have an effect similar to an ion-selective membrane (e.g., Bücker and Hördt, 2013). Strength and relaxation behavior of EDL polarization are influenced by background ion concentration in the pore water and surface charge density, among other factors (e.g., Lyklema, 2005). Importantly, the relaxation time relates to the spatial length scale of the polarization process and the ionic diffusion coefficient in the EDL, which may be different for Stern layer and diffuse layer polarization (e.g., Lyklema et al., 1983). The relationship between relaxation time and characteristic length scale for induced polarization in soils and sediments has been investigated in many studies (e.g., Titov et al., 2002; Binley et al., 2005; Kruschwitz et al., 2010; Revil and Florsch, 2010; Revil et al., 2014).

### 2.2 Electrical measurements

Electrical methods measure the conduction and polarization properties of a medium. In the frequency domain, the measured quantity is the complex-valued impedance, with the real (ohmic) part accounting for conduction, and the imaginary part accounting for polarization (capacitive) effects.

The electrical impedance,  $\hat{Z}$ , at a measurement (angular) frequency  $\omega$  is defined as the ratio of the complex voltage  $\hat{U}$  to the current  $\hat{I}$ , and can be represented by a real part  $Z'$  and an imaginary part  $Z''$ :

$$\hat{Z}(\omega) = \frac{\hat{U}(\omega)}{\hat{I}(\omega)} = Z'(\omega) + jZ''(\omega), \quad (1)$$

with  $j$  denoting the imaginary unit. The inverse of the impedance is the admittance  $\hat{Y}(\omega) = 1/\hat{Z}(\omega) = Y'(\omega) + jY''(\omega)$ . Impedances, or admittances, can be translated to effective material properties by means of a (real-valued) geometrical factor  $K$ , which takes into account the geometric

dimensions of the measurement (in particular electrode positions):

$$\hat{\rho}_a(\omega) = K \hat{Z}(\omega) = \frac{K}{\hat{Y}(\omega)}, \quad (2)$$

$$\hat{\sigma}_a(\omega) = \frac{\hat{Y}(\omega)}{K} = \frac{1}{K \hat{Z}(\omega)} = \frac{1}{\hat{\rho}_a(\omega)}, \quad (3)$$

with  $\hat{\rho}_a$  and  $\hat{\sigma}_a$  being the apparent complex resistivity and apparent complex conductivity, respectively. These quantities are referred to as “apparent” because they actually only represent the true properties if the medium under investigation is homogeneous. Otherwise, they represent an effective (average) value. Spatial discrimination of electrical properties can be achieved by the use of multiple measurements with different electrode locations, which also form the basis for tomographic processing (inversion), i.e., imaging.

Impedance measurements can be conducted using only two electrodes for a combined current- and voltage measurement, or by using four electrodes (quadrupole measurements, also called four-point spreads) with separate current and voltage electrode pairs. In the latter case, the contact impedance between electrode and medium, which becomes significant towards lower measurement frequencies, has practically no influence on the voltage measurement (e.g., Barsoukov and Macdonald, 2005).

### 2.3 Polarization of biomatter

Polarization phenomena of biomatter are commonly classified into three frequency regions with different polarization sources, namely the  $\alpha$ ,  $\beta$ , and  $\gamma$  regions (e.g., Schwan, 1957; Prodan et al., 2008). While overlapping, the low-frequency  $\alpha$  polarization is thought to extend into the lower kHz range, followed by the  $\beta$  polarization in the range up to about 100 MHz, and joined by the  $\gamma$  polarization at higher frequencies (e.g., Repo et al., 2012). Controlled by the mobility of the charge carriers, the  $\alpha$  range is assumed to be associated with electrochemical polarization (i.e., the build-up and relaxation of ionic concentration gradients such as those found in EDLs, in an electric, time-variable field); the  $\beta$  range by the Maxwell–Wagner polarization of composite media (e.g., Prodan and Prodan, 1999; Prodan et al., 2008); and the  $\gamma$  range by molecular, ionic, and atomic polarization. The different processes lead to different current flow paths within biomatter for different frequencies (Repo et al., 2012). These observations have been primarily made on cell suspensions and various kinds of tissue, which exhibit structures that are much more homogeneous than fully developed plant and root systems. Polarization processes in plant roots are assumed to originate among others in the cell membranes, the apoplast and the symplast (Repo et al., 2014). The frequency dependence of published multi-frequency measurements (e.g., Ozier-Lafontaine and Bajazet, 2005; Repo et al., 2014) indicates multiple length scales and associated structures as the origin of electrical polarization responses.

On a cellular, or multi-cellular level, much work has been conducted to gain information about the electrical surface characteristics of cells (cell structures). A Gouy–Chapman–Stern model relating surface charges to external ion concentrations has been formulated and subsequently improved (Kinraide et al., 1998; Kinraide, 1994; Wang et al., 2011). Using this model, ion activity at membrane surfaces can be computed and analyzed for the investigation of physiological effects. These and subsequent studies regarding ion toxicity and related surface electric potential have provided further evidence that certain surface potentials can be linked to physiological states and processes, e.g., ion availability and uptake (Wang et al., 2009, 2011, 2013; Kinraide and Wang, 2010). Li et al. (2015) estimated the electric potential at rice-root surfaces of macroscopic root segments using measurements of the electrokinetic zeta-potential. The zeta-potential is the experimentally accessible electric potential at a distance from the surface where slipping in the electrolyte occurs upon a flow-driving pressure gradient.

The EDL is the source of polarization responses in the low-frequency range usually measured with EIS/EIT. It is sensitive to physiological processes that affect ion (nutrient) availability in the vicinity of, and ion fluxes across, charged cell membranes. The key function of roots is the uptake of water and nutrients, which is highly dependent on nutrient availability, demand, and stress factors (e.g., Claassen and Barber, 1974; Delhon et al., 1995; Hose et al., 2001). Nutrient availability can influence water (and nutrient) transport within plant systems (e.g., Clarkson et al., 2000; Martínez-Ballesta et al., 2011), and nutrient availability within roots can fluctuate in response to certain depletion situations (e.g., Benlloch-González et al., 2010). Furthermore, the distribution of stress hormones such as abscisic acid (ABA) increases in response to stress situations, possibly inducing the aforementioned reactions (e.g., Schraut et al., 2005). The formation and properties of large-scale ion-selective structures such as endodermis and hypodermis are also directly influenced by the growth environment, and can change in response to external stress factors (Hose et al., 2001). In addition, Dalton (1995) noted that electrical polarization effects originate in the “active” parts of a root system only, which change according to age, nutrient availability, and other stress factors (see also Anderson and Hopmans, 2013).

The majority of studies concerning full root systems work with equivalent electrical circuit models to describe the measured signals of various biostructures (see Repo et al., 2012, and references therein). The scale and composition of these models vary considerably. For example, Dalton (1995) equates root segments with cylindrical capacitors, whose conducting plates are formed by the inner xylem and the fluid surrounding the root segment, with root cortex acting as a dielectric. Kyle et al. (1999) proposed a simplified model of cell polarization in root systems, in which the cell membrane acts as a dielectric between the conducting inner and outer regions of the cells, thus representing a classical capac-

itor. Equivalent circuit representations inherently depend on the assumed flow paths of the electric current. For instance, impedance measurements using the stem as one pole for current injection and the medium surrounding the roots as the other pole (as frequently being done, e.g., Chloupek, 1976; Dietrich et al., 2013; Repo et al., 2014) force the current to cross all radial layers of the roots. However, even for stem injection, equivalent circuit models considerably simplify the true electrical processes in the root and root–rhizosphere system, and it is questionable whether these models can be transferred between different experimental setups (as evident from the large number of slightly different models that were proposed, e.g., Dalton, 1995; Ozier-Lafontaine and Bajazet, 2005; Dietrich et al., 2013). A purely phenomenological analysis is made by Repo et al. (2014), who use a classification approach to analyze spectral impedance data measured on pine roots infested with mycorrhizal fungi.

#### 2.4 Working hypotheses

We propose to describe and interpret low-frequency (< 1 kHz) polarization processes in biomatter using concepts similar to those established for soils and rocks in recent years, under the assumption that the observed responses originate from the polarization of EDLs present in the biomatter. Accordingly, it should be possible to link the polarization magnitude to the average EDL thickness, which depends on the electric potential drop between the charged surface/membrane and the background ambient electrolyte, and link characteristic relaxation times to the length scales at which the polarization processes take place.

Given the current observations and understanding of electrical polarization processes in biomatter, as reviewed in the previous section, our hypotheses are as follows:

1. The magnitude of the low-frequency polarization response of roots is related to the overall surface area comprised by EDLs in the root–rhizosphere system, including the inner root structure. EDLs may form at Caspary strips (e.g., hypodermis and endodermis) and plasma membranes.
2. The characteristic relaxation times of the low-frequency polarization response of roots provide information on the length scales at which the polarization processes take place. While it is not clear to what extent a discrimination of specific polarization processes (e.g., plasma membrane polarization and polarization of the hypodermis) is possible, changes in the relaxation times should indicate changes in the length scale of the polarizing structures.
3. EDLs in the inner root system are influenced by ions (nutrients) in the sap fluid, EDLs at the outer root surface are influenced by ion concentrations in the external fluid. Thus, physiological processes that influence the

availability, usage, and translocation of ions directly influence the low-frequency polarization response.

4. Spectral EIT is a suitable non-invasive method to image and monitor magnitude and characteristic relaxation times of the low-frequency polarization response of root systems.

In the present study, we address the second part of hypothesis three, as well as hypothesis four. Hypotheses one and two are based on the synthesis of existing works, but can neither be validated nor invalidated by the present study.

### 3 Material and methods

#### 3.1 Electrical impedance tomography

The EIS (or SIP) method involves the measurement of impedances at multiple frequencies (usually in the mHz to kHz range). It can be extended by utilizing electrode arrays consisting of tens to hundreds of electrodes to collect numerous, spatially distributed four-point impedance measurements. From these data sets images of the complex conductivity (or its inverse, complex resistivity) can be computed using tomographic inversion algorithms (e.g., Kemna, 2000; Daily et al., 2005). This method is called complex conductivity (or complex resistivity) imaging or electrical impedance tomography (EIT), and refers to both single- and multi-frequency (spectral) approaches. EIT images are characterized by a spatially variable resolution, which decreases with increasing distance from the electrodes (e.g., Alumbaugh and Newman, 2000; Friedel, 2003; Binley and Kemna, 2005; Daily et al., 2005). The method's primary fields of application are in near-surface geophysics (e.g., Binley and Kemna, 2005; Daily et al., 2005; Revil et al., 2012) and medical imaging (e.g., Bayford, 2006).

Spectral EIT measurements presented in this study were conducted using the 40-channel EIT-40 impedance tomograph (Zimmermann et al., 2008), which was configured in a monitoring setup to acquire up to seven EIT data sets (frames) from a mini rhizotron per day.

##### 3.1.1 2-D forward modeling

Synthetic impedance data, required in the tomographic inversion process, were modeled using the finite-element (FE) forward modeling code of Kemna (2000). The code solves the Poisson equation for a 2-D complex conductivity distribution and 2-D source currents in a domain of given thickness (Flores Orozco et al., 2012b). At the boundaries of the 2-D modeling domain, no-flow Neumann conditions are imposed, which do not allow any current flow out of the modeling domain. Details of the implementation can be found in Kemna (2000).

A sketch of the FE grid (also used for the inversion and presentation of imaging results) resembling the rhizotron is

shown in Fig. 1b along with the position of 38 electrodes. The grid consists of 60 elements in the  $x$  direction, and 157 elements in the  $z$  direction (9420 elements in total).

### 3.1.2 2-D tomographic inversion

Complex conductivity images at multiple measurement frequencies were computed using the smoothness-constraint inversion code of Kemna (2000). The code computes the distribution of complex conductivity  $\hat{\sigma}$  (expressed in either magnitude ( $|\hat{\sigma}|$ ) and phase ( $\phi$ ) or real component ( $\sigma'$ ) and imaginary component ( $\sigma''$ )) in the 2-D ( $x, z$ ) image plane from the given set of complex transfer impedances  $\hat{Z}_i$  (expressed in magnitude ( $|\hat{Z}_i|$ ) and phase ( $\varphi_i$ )) under the constraint of maximum model smoothness. Log-transformed impedances and log-transformed complex conductivities (of the individual elements of the grid) are used as data and model parameters, respectively, in the inversion.

The iterative, Gauss–Newton type of inversion scheme minimizes an objective function composed of measures of data misfit and model roughness. The data misfit is weighted by the (real-valued) magnitudes of individual, complex-valued data errors (see Kemna, 2000), which, however, are dominated by the resistance errors since the phase values are relatively small for the measurements considered here. Therefore the resistance error model (LaBrecque et al., 1996)

$$\Delta|\hat{Z}_i| = a|\hat{Z}_i| + b \quad (4)$$

can be used in the complex inversion for the weighting of complex data (including the phase), with  $\Delta|\hat{Z}_i|$  being the error of impedance magnitude (resistance)  $|\hat{Z}_i|$ ,  $a$  a relative error contribution, and  $b$  an absolute error contribution. For more details on the inversion scheme we refer the reader to Kemna (2000). The inversion is separately performed for each frequency of the given data set.

### 3.2 Debye decomposition

The Debye decomposition (DD) approach (e.g., Uhlmann and Hakim, 1971; Lesmes and Frye, 2001) was used to analyze the complex conductivity spectra recovered from the multi-frequency EIT inversion results. The approach yields integral parameters describing the spectral characteristics of the SIP signature. The complex conductivity spectrum is represented as a superposition of a large number of Debye relaxation terms at relaxation times  $\tau_k$  (suitably distributed over the range implicitly defined by the data frequency limits; see Weigand and Kemna, 2016):

$$\hat{\sigma}(\omega) = \sigma_\infty \left[ 1 - \sum_k \frac{m_k}{1 + j\omega\tau_k} \right], \quad (5)$$

with  $\sigma_\infty$  being the (real-valued) conductivity in the high-frequency limit, and  $m_k$  the  $k$ th chargeability, describing the

relative weight of the  $k$ th Debye relaxation term in the decomposition. The chargeabilities  $m_k$  at the different relaxation times  $\tau_k$  form a relaxation time distribution (RTD), from which the following descriptive parameters are computed (e.g., Nordsiek and Weller, 2008):

- The normalized total chargeability  $m_{\text{tot}}^n$  is a measure of the overall polarization reflected in the spectrum (e.g., Tarasov and Titov, 2013; Weigand and Kemna, 2016):

$$m_{\text{tot}}^n = \sigma_0 \sum_k m_k, \quad (6)$$

with  $\sigma_0$  being the (real-valued) conductivity in the low-frequency limit.

- The mean logarithmic relaxation time  $\tau_{\text{mean}}$  represents a weighted mean of the RTD:

$$\tau_{\text{mean}} = \exp \left( \frac{\sum_k m_k \log(\tau_k)}{\sum_k m_k} \right). \quad (7)$$

- The uniformity parameter  $U_{60,10}$  describes the frequency dispersion of the spectrum:

$$U_{60,10} = \frac{\tau_{60}}{\tau_{10}}, \quad (8)$$

with  $\tau_{10}$  and  $\tau_{60}$  being the relaxation times at which the cumulative chargeability reaches 10 and 60 %, respectively, of the total chargeability sum.

The implementation of Weigand and Kemna (2016) was used for the DD analysis. The iterative inversion scheme balances between (error-weighted) data fitting and smoothing requirements.

### 3.3 Experimental setup

#### 3.3.1 Rhizotron

The experiment was conducted using a mini-rhizotron with the dimensions of 30 cm width, 78 cm height, and 2 cm thickness, and a transparent front plate (Fig. 1). The front of the rhizotron is equipped with 38 brass pins of 5 mm diameter as electrodes, which do not extend into the rhizotron's inner volume. A growth lamp was installed above the rhizotron and turned on during daylight hours.

#### 3.3.2 Plant treatment

Oilseed plants had been grown in nutrient solution prior to the experiment. To increase the root mass, three plants were tied together and centrally placed at the top of the rhizotron (Fig. 1), which had been filled with tap water before. No water was added to the rhizotron during the experiment, nor was the water in the rhizotron disturbed in any way. Thus, it is possible that at some point anaerobic conditions manifested.

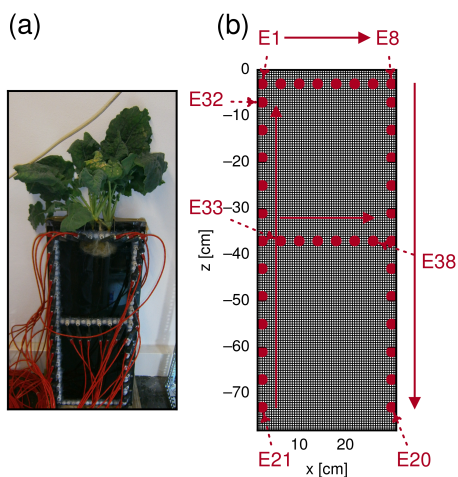


**Figure 1.** (a) Experimental setup of plant root systems in water-filled rhizotron. (b) Corresponding finite-element grid used for electrical modeling and imaging. Red dots indicate position of electrodes. Red arrows indicate the ascending order of electrode numbering, some of which are marked using the notation E1–E38.

### 3.3.3 Data acquisition

Over the course of 3 ays, 21 EIT data sets at 35 frequencies between 0.46 Hz and 45 kHz were collected in regular intervals, starting right after the placement of the plant system in the rhizotron. A total of 1158 quadrupoles were measured for each data set, involving 74 individual current injections (plus 767 reciprocal configurations, where current and voltage electrode pairs are interchanged, for quality assessment), requiring less than 4 h acquisition time. These quadrupoles consisted mostly of skip-0 and skip-2 (numbers of electrodes between the two electrodes used for current injection and voltage measurement, respectively) dipole–dipole configurations, as well as quadrupoles with current electrodes on opposite sides (left and right) of the rhizotron and skip-0 voltage readings.

## 3.4 Data processing

### 3.4.1 Selection of impedance data

The inversion scheme assumes normally distributed and uncorrelated data errors and is very sensitive to outliers (e.g., LaBrecque and Ward, 1990). Outliers are usually associated with low signal-to-noise ratios or systematic errors due to missing or bad electrode contacts. Outliers can either be removed from the data set prior to inversion or accounted for by sophisticated, “robust” inversion schemes (LaBrecque and Ward, 1990). In these robust schemes, the weighting of individual data points is iteratively adapted, which can lead to a reduction of spatial resolution as well as recovered contrast in the imaging results. However, usually this does not change the qualitative results of the inversion. In the present

study, we sought to analyze data across the frequency and time domains, which requires a careful and consistent analysis of the inversion data. Thus, to prevent introducing unnecessary variations between time steps and frequencies, we opted to remove outliers using the criteria described below and use individual, but consistent, data weighting schemes for all measurements.

The measured impedance data (also referred to as “raw data”, in contrast to complex conductivity data recovered from the imaging results, referred to as “intrinsic data”) were screened (filtered) for outliers and faulty data according to multiple criteria: First, outliers were identified for each frequency and time step and removed from the data set. Due to the underlying physical principles, EIT measurements usually do not show strong variations when electrode positions are only slightly shifted. The exception here is measurements with electrodes located close to the plant stem system, where a very localized anomalous response is expected in the data. Accordingly, care was taken not to remove these data as outliers. Second, following this selection process, only impedance spectra were kept that retained more than 90 % of the original data points below 300 Hz and showed consistency over several time steps. Third, to avoid errors due to electromagnetic coupling effects (e.g., Pelton et al., 1978; Zhao et al., 2013), only data below 220 Hz were considered for the imaging. Fourth, measurements at 50 Hz were discarded due to powerline noise.

The applied data selection criteria resulted in small variations in the number of measurements actually used for the inversions for the different time steps, ranging between 530 and 555 measurements per data set and frequency. The average injected current strength of the measurements at each time step increased slightly over time from approximately 1.0 to 1.2 mA.

### 3.4.2 Correction of impedance data for imperfect 2-D situations

Since the electrodes do not extend across the entire depth (i.e., horizontal direction perpendicular to the image plane) of the rhizotron, the electric current and potential field distributions in the rhizotron are not perfectly 2-D, as is assumed in the forward modeling. Therefore measurements were conducted on a rhizotron solely filled with tap water of known conductivity. By comparing the latter with the apparent conductivity (Eq. 3) derived from the measured impedance and the numerically determined geometric factor (obtained from running the forward model for a homogeneous case) for each measurement configuration, correction factors were computed and applied to all measured impedances.

From a theoretical point of view, these correction factors are independent of the conductivity value of a homogeneous distribution since measured resistance and resistivity (inverse of conductivity) are linearly related for a homogeneous distribution. Significant changes in the correction factors can

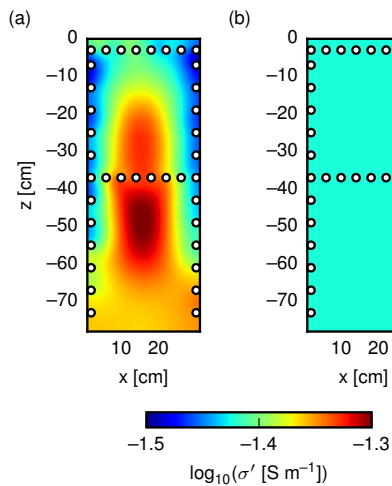


**Figure 2.** EIT inversion results (real component of complex conductivity) for measurements on a rhizotron filled with water of known conductivity ( $375 \mu\text{S cm}^{-1} = 10^{-1.43} \text{ S cm}^{-1}$ ) without (a) and with (b) correction of the impedance data for the imperfect 2-D situation.

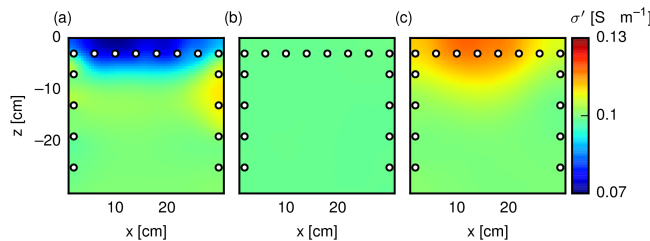
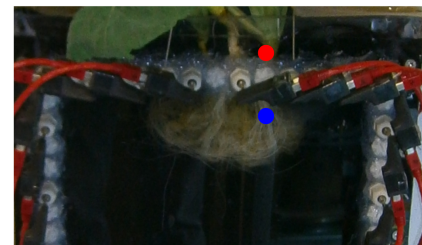


**Figure 3.** EIT inversion results (real component of complex conductivity) obtained from synthetic data using a modeling grid in the inversion with a (a) 1.5 cm lower, (b) identical, and (c) 1.5 cm higher position of the top boundary compared to the grid (forward model) used to compute synthetic measurements. The forward model was homogeneously parameterized with a conductivity distribution of  $0.1 \text{ S m}^{-1}$ . Only the upper part of the modeling domain (rhizotron) is shown. Electrode positions and measurement configurations are the same for all three cases.

only occur for strong spatial conductivity variations, in particular across the thickness of the rhizotron (2-D/3-D effects). However, even if present, such effects in the correction factors would primarily result in inaccuracies in the inverted conductivity magnitude image, while the conductivity-phase image and also the DD-derived spectral parameters (total chargeability, relaxation time) are relatively robust against magnitude, i.e., correction factor, errors. We therefore, for the small to moderate conductivity variations observed in the experiment in the upper region of the rhizotron, assume that the conducted calibration survey, i.e., one universal set of correction factors, was actually sufficient.

In Fig. 2 the effect of this correction procedure on the EIT inversion result is shown. Without correction the obtained image exhibits an artificial pattern (Fig. 2a), while with cor-



(a)

Day 1



(b)

Day 3



(c)

**Figure 4.** Photographs of the oilseed plants during the experiment: (a) close-up of the root systems in the rhizotron container, (b) day 1 and (c) day 3. The colored dots in (a) indicate the approximate position at which intrinsic signatures, recovered from tomographic inversion results, are investigated; red dot: stem area; blue dot: fine root area.

rection a practically homogeneous distribution is recovered, in agreement with the conductivity of the tap water (Fig. 2b).

The inversion was conducted using the error parameter values  $a = 0.5\%$  and  $b = 0.012\Omega$  (see Eq. 4). These values were found to be appropriate and were also used in the inversions, of which the results are shown in the following.

### 3.4.3 Adaptation of modeling domain to changing water table

Due to evaporation and root water uptake the water table fell by ca. 2 cm over the course of the monitoring experiment. This was not problematic in terms of electrode contact as electrodes always remained in the water. However, the changing water table has to be accounted for in the EIT inversion by means of an adapted modeling domain, i.e., by adapting the position of the top boundary of the FE modeling grid, where no-flow conditions are assumed. Otherwise, as we checked in numerical experiments, significant artifacts appear in the inversion results (Fig. 3).

From the known water tables at the beginning and end of the experiment, and the average time when each EIT data set was collected, the positions of the top boundary of the individual grids used for the inversion of each data set were determined by linear interpolation.

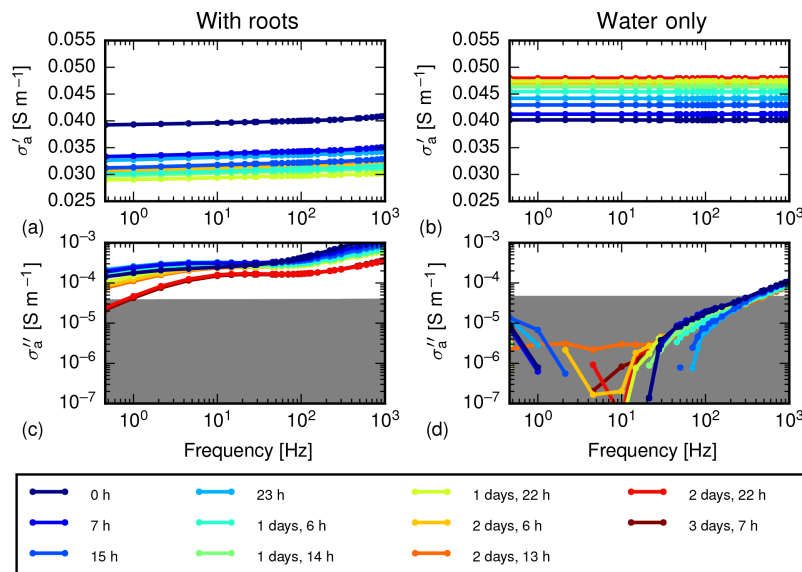


**Figure 5.** Temporal evolution of raw data spectra, plotted as real (**a, b**) and imaginary (**c, d**) components of apparent complex conductivity (Eq. 3) for two example measurement configurations: (**a, c**) current injection between electrodes 3 and 4, and voltage measurement between electrodes 5 and 6 (quadrupole located directly above the root system, i.e., response “with roots”); (**b, d**) current injection between electrodes 34 and 35 and voltage measurement between electrodes 36 and 37 (quadrupole located in an area relatively far away from the root system, i.e., “water-only” response). For electrode numbering, see Fig. 1b. Blue indicates early measurements, while later ones are shown in red. Values of  $\sigma''$  that lie below the measurement accuracy of the system (1 mrad phase shift at 1 kHz for water; see Zimmermann et al., 2008) are indicated by gray areas.

### 3.4.4 Analysis of spectral imaging results

The spectral imaging results were analyzed by means of pixel-wise application of the Debye decomposition scheme. As water exhibits no significant polarization response in the examined frequency range, the area free of roots from 20 to 78 cm depth of the rhizotron was used to quantify a  $m_{\text{tot}}^n$  threshold value below which polarization is considered insignificant. Based on this threshold value all images of the spectral parameters obtained from the Debye decomposition, including the top 20 cm of the rhizotron, were partitioned into pixels with and without significant polarization. The observed polarization can be fully attributed to the root system (no polarization is expected from the surrounding water in the examined frequency range) and thus the corresponding pixels delineate polarizable areas of the root system, which we refer to as the root pixel group.

To analyze the temporal evolution of the overall root system polarization (in terms of normalized total chargeability) the root pixel group was determined for the first time step, and then kept fixed for the following time steps. Relaxation times, however, can only be reliably extracted from SIP signatures if they show significant polarization. Therefore, for the relaxation time analysis (in terms of mean relaxation time and uniformity parameter) the root pixel groups were determined for each time step individually.

## 4 Results

### 4.1 Physiological response

Photographs of the plant systems at the beginning and the end of the experiment are shown in Fig. 4. As is evident from the photographs, the plants significantly reacted to the nutrient stress situation (and possibly anaerobic conditions) and degraded over time. The root systems extended down to a depth of approximately 13 cm, with an approximate maximum lateral extension of 13 cm (see Fig. 1).

### 4.2 Impedance spectra

In Fig. 5 the temporal evolution of the raw data spectra in terms of apparent complex conductivity (Eq. 3) is shown for two example measurement configurations: a quadrupole with electrode pairs on both sides of the rhizotron located directly above the root system, i.e., with sensitivity to the root system and a quadrupole with electrodes from the horizontal electrode line at 37 cm depth, i.e., located relatively far away from the root system and thus sensitive only to the water. The real component of apparent complex conductivity shows a smooth, consistent behavior across the time and frequency domains for both responses, “with roots” and “water-only” (Fig. 5a, b). However, the conductivity decreases for the quadrupole around the root system, while it increases in the “water-only” quadrupole. The imaginary components, i.e.,

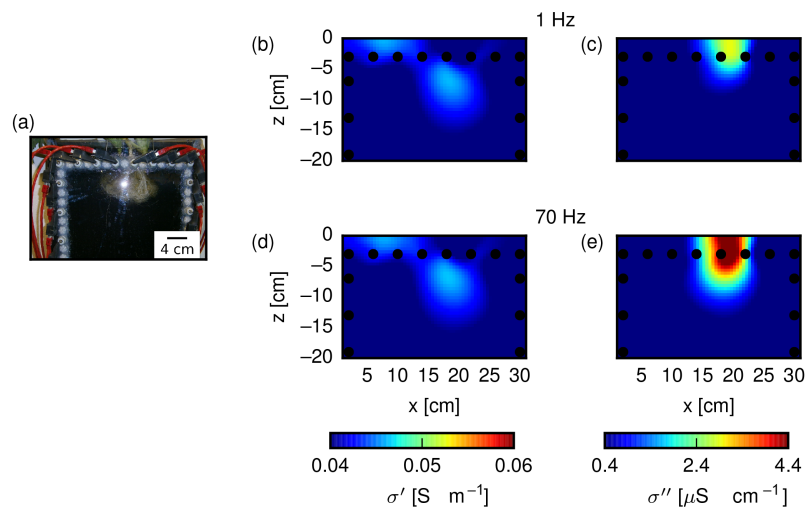


**Figure 6.** Single-frequency inversion results in terms of real (**b**, **d**) and imaginary (**c**, **e**) components of complex conductivity for 1 Hz (**b**, **c**) and 70 Hz (**d**, **e**) at the first time step. The photograph of the root system at this time (**a**) shows the same area of the rhizotron as the inversion results.

the polarization responses, with roots (Fig. 5c) are also consistent and show changes, especially in the lower-frequency range, over time. The water-only measurements, on the other hand, only exhibit negligible polarization responses, likely dominated by measurement errors and noise (Fig. 5d). The polarization magnitudes, on the one hand, lie well below the signal threshold that can be reliably measured with the EIT-40 system (Zimmermann et al., 2008); the jittery shape of these signatures (Fig. 5d) is attributed to the logarithmic scale of the plot. On the other hand, measured root signatures lie clearly above the measurement threshold of the system (Fig. 5c).

#### 4.3 Single-frequency imaging results

The spatial variability of the electrical response was assessed using the complex conductivity imaging results, i.e.,  $\sigma'$  and  $\sigma''$ , at the first time step for the two frequencies 1 and 70 Hz (Fig. 6). Only weak variations in the real component (in-phase conductivity) can be observed at the location of the root system (Fig. 6b, d). However, a significant polarization response in the imaginary component (Fig. 6c, e) coincides with the extension of the root system. The frequency dependence previously found in the apparent complex conductivity spectra (see Fig. 5) is also revealed in the imaging results, with a stronger response at 70 than at 1 Hz. It manifests both in signal strength and in the spatial extension of the polarizable anomaly associated with the root system.

#### 4.4 Complex conductivity spectra recovered from imaging results

Complex conductivity spectra were extracted from the multi-frequency imaging results at three locations: near the stem

area of the root system, from the lower area of the root system, and from the lower half of the rhizotron, where no root segments were present. The two locations near the root system are indicated in Fig. 4a. Thus, these locations represent areas with relatively thick root segments, thin root segments, and no root segments (water only) at all. Figure 7 shows the temporal evolution of the spectral response for the three locations. The real component of complex conductivity ( $\sigma'$ ) increased over the course of the experiment for all three locations (Fig. 7a–c). The imaginary component of complex conductivity ( $\sigma''$ ) reveals a frequency-dependent polarization response at the root segment locations for all time steps (Fig. 7d, e). The polarization magnitude decreases over time, and changes in the shape of the spectra can be observed for later time steps. These changes are most pronounced for the location near the stem (Fig. 7a). The polarization signatures recovered at the bottom of the rhizotron (water only) show an amount that is almost 2 orders of magnitude smaller (Fig. 7f) compared to those in the root system areas; they contain more noise and do not exhibit a clear frequency trend.

#### 4.5 Debye decomposition of recovered complex conductivity spectra

The Debye decomposition scheme was applied to the complex conductivity spectra recovered from multi-frequency EIT to quantify the overall polarization (normalized total chargeability  $m_{\text{tot}}^n$ ) and the characteristic relaxation time (mean relaxation time  $\tau_{\text{mean}}$ ), as well as the uniformity parameter  $U_{60,10}$ . By means of this analysis, the intrinsic spectra can be assessed with respect to the magnitude and shape of the polarization response for all pixels at each time step. Figure 8 shows a decomposition result of a pixel signature from the stem area for the first time step, corresponding to

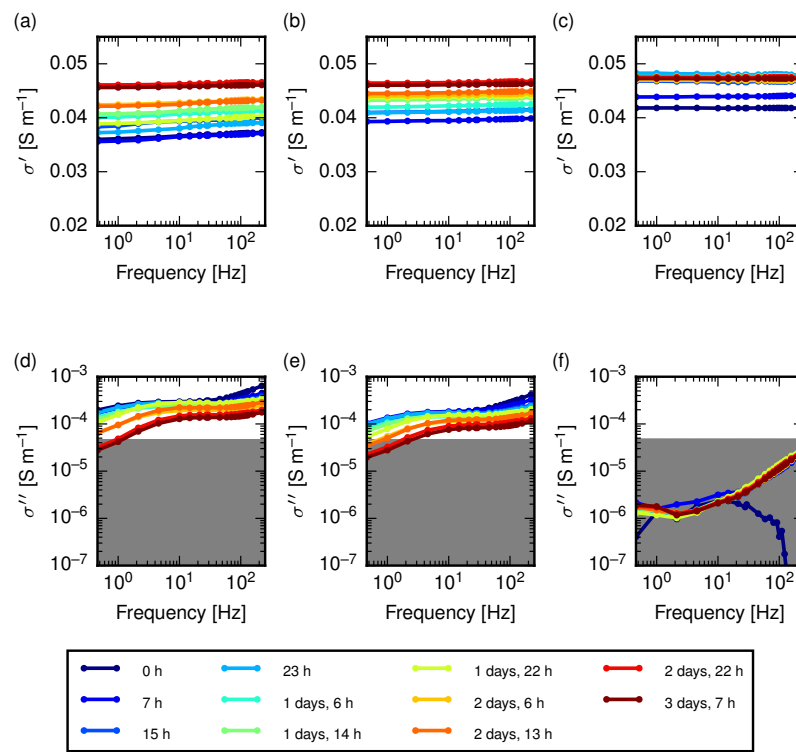


**Figure 7.** Intrinsic complex conductivity spectra (in terms of real component  $\sigma'$  and imaginary component  $\sigma''$ ) for all time steps (indicated by color of the curves) recovered from the multi-frequency inversion results at different locations in the rhizotron: (a, d) stem area ( $x$  position: 20.25 cm;  $z$  position:  $-0.75$  cm); (b, e) bottom of the root system ( $x$  position: 20.25 cm;  $z$  position  $-6.25$  cm); (c, f) water-only location ( $x$  position: 20.25 cm;  $z$  position:  $-50.25$  cm). Positions for (a and d) and (b and e) are also indicated in Fig. 4a. Values of  $\sigma''$  that lie below the measurement accuracy of the system (1 mrad phase shift at 1 kHz for water; see Zimmermann et al., 2008) are indicated by gray areas.

the spectrum plotted in Fig. 7a, d at “0 h” (dark blue curve). The complex conductivity spectrum was fitted by means of 96 Debye relaxation terms (Fig. 8a), yielding a relaxation time distribution (RTD) (Fig. 8b), from which  $\tau_{\text{mean}}$ ,  $\tau_{10}$ , and  $\tau_{60}$  can be determined (Fig. 8a, b). We note that  $\tau_{\text{mean}}$  does not coincide with the RTD peak, which only happens if the RTD shows a perfect symmetry (in log scale), which is not the case here.

#### 4.6 Images of spectral parameters obtained from Debye decomposition

Images depicting the DD-derived total polarization ( $m_{\text{tot}}^n$ ) results of the complex conductivity spectra (obtained from multi-frequency EIT) for selected time steps are presented in Fig. 9. The extension of the root system against the surrounding water (characterized by low polarization) is clearly delineated in the images, and a continuous decrease in polarization strength is observed over time.

For further analysis, the complex conductivity spectra (also referred to as pixel spectra) were classified into two categories, with and without root segments, as described in Sect. 3.4.4. The resulting “root system spectra” were then processed separately, and care was taken that the selected

spectra exhibit a sufficiently strong and consistent polarization response to allow a reliable relaxation time analysis. Figure 10 shows the comparison of the  $m_{\text{tot}}^n$  results for the first time step with the extension of the root system according to the photograph. The root system area reconstructed from the spectral EIT results shows a good agreement with the known outer boundaries of the root system. Systematic changes in the overall root system response were analyzed by averaging the  $m_{\text{tot}}^n$  pixel values in the root system zone (Fig. 11). This average polarization response shows a steady decrease over time.

Images of the DD-derived mean relaxation time  $\tau_{\text{mean}}$  are presented in Fig. 12 for selected time steps. Spatial variations within the root system zone can be observed for each time step, as well as changes between time steps. A general trend from larger relaxation times (up to 18 ms) to smaller relaxation times (down to 9 ms) over the course of the experiment is noticeable. Corresponding images of the uniformity parameter  $U_{60,10}$  are shown in Fig. 13. Observed variations within images and between time steps indicate changes in the shape of the pixel spectra. Values approaching 1 indicate a stronger spectral dispersion, i.e., a focusing of the spectral polarization response in a narrower frequency band.

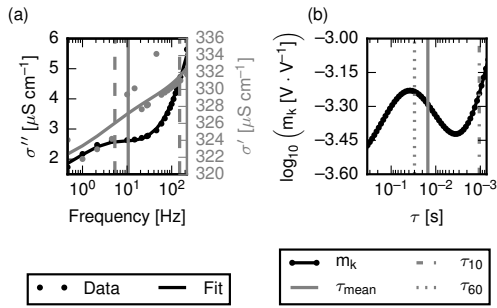


**Figure 8.** Debye decomposition (DD) of the recovered complex conductivity spectrum for a pixel from the stem area with maximum polarization response (see, Figs. 5 and 7): **(a)** complex conductivity (gray: real component; black: imaginary component) from spectral EIT (dots) and fitted DD response (solid curves); **(b)** corresponding relaxation time distribution. Vertical gray solid lines indicate  $\tau_{\text{mean}}$ , and the dashed vertical lines indicate  $\tau_{10}$  and  $\tau_{60}$ , respectively.

## 5 Discussion

The following discussion is divided into two parts: the biological discussion of the experiment and the assessment of the geophysical methodology for crop root investigations.

### 5.1 Biological interpretation

In the course of the experiment, a conductivity increase is observed (Fig. 7a–c), which originated at the bottom of the rhizotron and continuously migrated upwards (see S1 in the supplement for conductivity images of the whole rhizotron). This spatial pattern rules out the root system as the cause of the conductivity increase, and we attribute it to the dissolution and subsequent upwards diffusion of impurities at the bottom of the rhizotron frame. While a certain influence on the spectral parameter results (Figs. 9 and 12) is possible, we believe the impact to be relatively small for two reasons: First, the observed time evolution of  $m_{\text{tot}}^n$  shows changes more or less centered around the stem region, not following the distribution pattern of the conductivity increase; second, we observe changes in the spectral behavior of the signatures (in terms of  $\tau_{\text{mean}}$ ), which can not be explained by an increase in conductivity. However, in future experiments the background conditions should be monitored and the plant only inserted once equilibrium of the system has been reached.

The physiological response of the root system to the imposed nutrient deprivation and possible anaerobic conditions is reflected by a decreasing overall polarization response (Figs. 9 and 11). Note that it is highly unlikely that the dropping water table caused this decrease in polarization, as more current is forced through the main bulk of the root system with the dropping water table. Thus, it should actually increase the polarization response, assuming that this response does not change due to physiological reactions in the root system. Note that the water table always remains above the

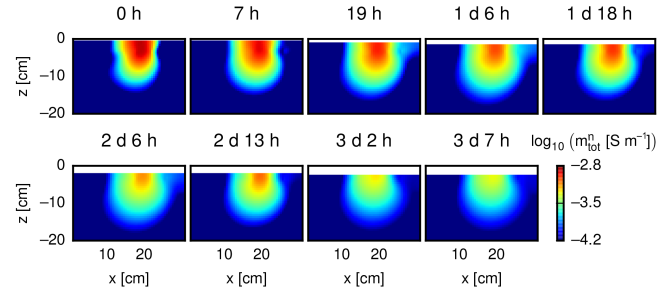


**Figure 9.** Spatial distribution of DD-derived parameter  $m_{\text{tot}}^n$  for selected time steps. The top boundary is adjusted according to the estimated water table for each measurement time.

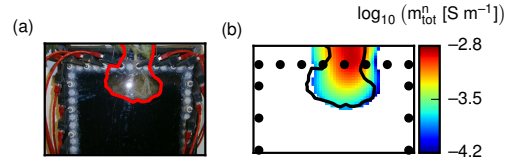


**Figure 10.** Comparison of root extension inferred from the photograph **(a)**, indicated by overlaid solid lines, and **(b)**  $m_{\text{tot}}^n$  results for the first time step. In **(b)** only pixels from the root zone, i.e., pixels with a polarization response above the identified  $\sigma''$  threshold value, are plotted.

actual root system and only drops in the stem area. We attribute the observed decrease in polarization to a general weakening of the EDLs present in the root system. The cause of this EDL weakening can be manifold and can not be isolated in this study. In the following, we shortly discuss two (possibly superimposing) approaches to interpretation.

The first approach is to consider ion (nutrient) concentration in the fluid phase of the EDL. Shoot–root systems represent a hydraulically connected system whose water potential is primarily controlled by water transpiration at the leaves. In the case of intact hydraulic connectivity in the plant, a decrease in water potential due to transpiration causes water and solute uptake by the roots, and water and solute flow from the roots to the leaves (Tinker and Nye, 2000). While it is possible that solutes were taken up by the plant in our experiment, no nutrients were available to the plant. Accordingly, for our experiment we expected that the root regions farther away from the stem, that is, the regions with the highest water potentials, were depleted of nutrients first, as the available nutrients were translocated to the stem and the leaf areas, following the (negative) water potential gradient. Plants can sense, and react to, stress situations and can initiate changes in solute transport and hydraulic membrane conductivity properties (e.g., Clarkson et al., 2000; Schraut et al., 2005), especially if dynamic responses are considered. As a result, without being able to pinpoint the exact cause, the ion concentration could have decreased in the vicinity of cell membranes in these depleted areas, leading to a weakening

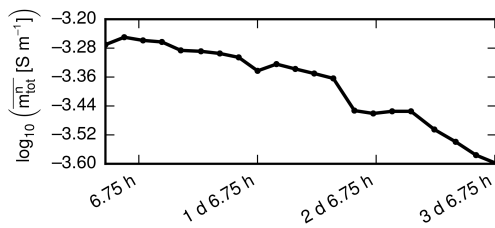


**Figure 11.** Mean value of DD-derived total chargeability  $m_{\text{tot}}^n$  plotted vs. time after start of the experiment. Average values were computed based on all pixels belonging to the root system zone.

of associated EDLs, in turn implying a decreased polarization response. The second approach is to consider changes in the electrical surface characteristics of cell membranes in reaction to the imposed physiological stress situation. These surface characteristics could have changed in response to certain active triggers, such as stress hormones, or as a result of balancing processes across the membranes. In light of these considerations, the stem should retain a more stable electrical polarization since it is likely not affected as much by physiological responses as the other, smaller, root segments (in terms of larger nutrient storage capability, better air availability, and general metabolic activity). This is consistent with the time-lapse imaging results, which show more stable polarization responses in the stem area (Fig. 9).

Another indication of the physiological stress response is the changes in the shape of the spectra (Figs. 12 and 13). Relative changes in the relaxation time contributions suggest changes in the underlying structures that control the polarization response at certain time steps. These changes might be related to new or ceased ion fluxes and their varying pathways within the root systems, as well as to varying surface charges at various structures such as the endodermis. If these structures change, or break down, in response to stress situations, corresponding changes in the electrical properties can be expected. However, given its spatial resolution limits, EIT does not allow one to distinguish these different structures directly.

Assuming that relaxation times can be linked to length scales of the underlying polarization processes, the observed signatures indicate multiple polarizable structures. However, the methodology applied here prevents further investigations in this direction. In contrast to most of the existing studies, we did not inject current directly in the stem, and correspondingly the explicit current pathways are much less defined in our approach. This prevents (at this stage) a simple formulation of an equivalent lumped electrical circuit model. Comparison of measurements using the procedure presented here with a stem-injection approach could, however, help to elucidate the origin of polarization and its length-scale characteristics. Current injection into the stem forces the current to flow through the root system and through all radial layers of the root segments, and thus a stronger polariza-

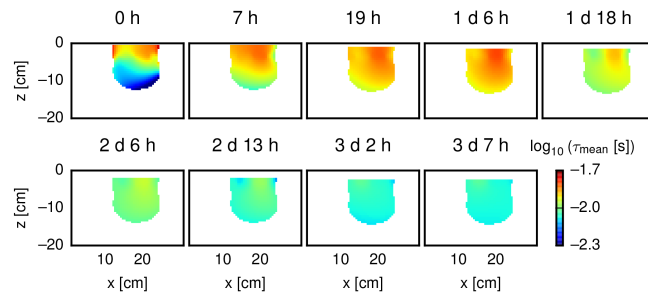


**Figure 12.** Spatial distribution of the DD-derived parameter,  $\tau_{\text{mean}}$ , for selected time steps. Only pixels belonging to the root system zone are plotted. Masked (white) pixels were classified as water. The top boundary is adjusted according to the estimated water table for each measurement time.

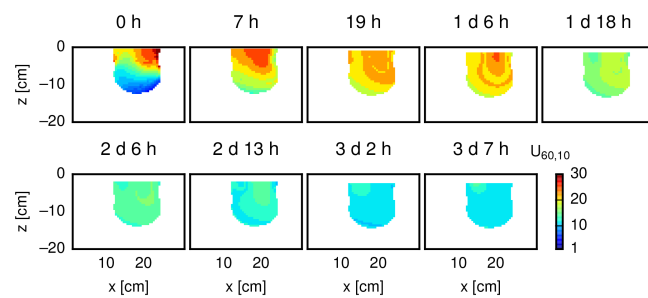


**Figure 13.** Spatial distribution of the DD-derived parameter,  $U_{60,10}$ , for selected time steps. Only pixels belonging to the root system zone are plotted. Masked (white) pixels were classified as water. The top boundary is adjusted according to the estimated water table for each measurement time.

tion response from inside the root segment can be expected, as well as the polarization of additional membrane structures. Additional experiments could focus on establishing relationships between recovered spectral polarization parameters and root-specific parameters, such as surface area and root length density. The use of sophisticated electrical models, coupled to existing macroscopic root development and nutrient uptake models (e.g., Dunbabin et al., 2013; Javaux et al., 2013), could provide further insight to identify the key processes that control the electrical polarization signatures of root systems. While this study focused on establishing the EIT methodology for crop root research, in future studies, physiological plant parameters such as leaf transpiration rates, which could help to identify the key processes that control electrical polarization signatures, should also be monitored.

As already pointed out by Repo et al. (2012), single-frequency measurements are of limited value to determine electrical polarization properties of root systems, both in terms of spatial distribution and polarization strength, and this finding is supported by our spectral EIS results (Figs. 5, 7, 12, and 13). This becomes even more obvious when interpreting the polarization signature as an EDL response,

which typically exhibits a strong frequency dependence. It should be noted that the frequency range analyzed here in an imaging framework (0.46 to 220 Hz) does not cover the full bandwidth that could be, in principle, measured with the presented setup, and corresponding advances are within easy reach (e.g., Huisman et al., 2015). However, reliable measurements at lower and higher frequencies will require careful adaptations in measurement and data processing procedures.

The classification of image pixels into two classes cannot, and should not, be treated as a universal analysis procedure. For the simple conditions in this experiment a clear distinction between the root system area and the surrounding medium could be made, which facilitated the assessment of the method (e.g., Fig. 11), and can potentially be used for further experiments with root systems in aqueous solutions. However, the primary results of this study do not rely on this specific classification, and likewise soil-based experiments could be conducted with the measurement setup.

This study does not involve any kind of granular substrate and thus excludes possible influences from such a background material. In fact, significant additional electrical polarization can be expected when soil surrounds the root system, which will superimpose on the root system response. Organic matter and micorrhiza may also contribute to the overall electrical signature. Finally, a variable water content can significantly influence the electrical response of the soil and the root system, either directly by influencing present EDLs or indirectly by inducing physiological processes such as nutrient uptake, which in turn can affect the electrical signatures of the EDLs.

## 5.2 Geophysical methodology

The observed polarization response of the root system is relatively weak and its measurement requires a corresponding measurement instrument accuracy. This accuracy is provided by the EIT-40 tomograph that was used in this study (Zimmermann et al., 2008). The high accuracy of the instrument was also recently demonstrated in an imaging study on soil columns (Kelter et al., 2015).

If fixed data weighting is used, which we believe would produce more reliable and consistent results for multi-frequency time-lapse data, data selection, i.e., filtering, becomes a relevant step in the processing pipeline before the inversion and subsequent spectral analysis. While it is common to remove outliers from geophysical data prior to inversion, filtering becomes challenging if multiple time steps are to be analyzed consistently. The number of retained data points varied slightly between time steps, although the same filtering criteria were applied. This can be explained by data noise and varying contact impedances at the electrodes. However, data quality was sufficient enough to produce consistent imaging results for all time steps and frequencies, as is evident from the impedance spectra (Fig. 5).

Another important issue is the data processing flow in the imaging framework, coupled with the spectral analysis based on the Debye decomposition. The inversion algorithm produces spatially smooth images; however, the images were computed for each frequency separately, and thus no smooth variation between adjacent frequencies is enforced in the inversion, although physically expected. Corresponding inversion algorithms have been developed recently (Kemna et al., 2014; Günther and Martin, 2016) and could lead to a further improvement of the multi-frequency imaging results. However, a similar constraint is introduced by the Debye decomposition, where smoothness is imposed along the relaxation time axis, which directly corresponds to the frequency axis. Minor noise components can thus be expected to be smoothed out both spatially and spectrally.

EIT applications in pseudo-2-D rhizotron containers require specific processing steps. The determination and testing of correction factors accounting for modeling errors due to an imperfect 2-D situation (Fig. 2) are as important as the correct representation of the rhizotron in terms of the FE grid underlying the inversion process (Fig. 3). Not taking these aspects into account can produce artifacts in the imaging results that can easily be misinterpreted in biological terms. Similarly, data errors should not be underestimated, as this can also produce misleading imaging results when data are overfitted (e.g., Kemna et al., 2012). Contrarily, an overestimation of data errors can mask information present in the data. Among other analysis steps, raw (impedance) data and imaging (complex conductivity) data should be checked for consistency and plausibility by taking into account the much lower spatial resolution of the raw data (see Figs. 5 and 7).

Electrical imaging results exhibit a spatially variable resolution, which usually decreases as the distance from the electrodes increases. One could question such a method's usefulness if the resolution cannot be clearly determined. Nonetheless, even limited spatial information allows for a distinction of polarizing and non-polarizing regions in the investigated object. This is not possible with spectroscopic measurements, and so it is even more difficult to analyze spatially distributed root systems with measurements such as these. We suspect that some of the reported inconsistencies in electrical capacitance relationships with biological parameters (e.g., Kormanek et al., 2015, and references therein) can be ascribed to missing spatial information in the measurement data. The resolution of EIT is not sufficient to image microscopic current flow paths in the root system, but the imaged macroscopic electrical properties can be compared for different regions of the root system, for instance the (older) top part of the root system compared to the younger lower part. Future improvements in experimental setups (electrode distribution and spacing) and measurement configurations will most probably lead to increased spatial resolution.

Another advantage of the EIT approach presented in this study is the possibility of arbitrarily placed electrodes (as long as the resulting geometrical arrangement allows for a

sufficient measurement coverage of the root system), in contrast to using stem electrodes as commonly done in previous studies. If the stem of a plant is used to inject current into the root system, measurements, and resulting correlations to biological parameters, are highly sensitive to the electrode position above the stem base (Dalton, 1995; Ozier-Lafontaine and Bajazet, 2005). Another problem is that electrodes can not be inserted into the stem if damage to the plant is to be avoided. However, injections can also be realized by use of non-invasive clamps.

The timescale of the physiological response to be monitored is also important for the experimental design. It took approximately 3.5 h to complete a single time frame of the spectral EIT measurements presented here. Thus, physiological processes taking place on a shorter time span cannot be resolved. Reducing the data acquisition time can be achieved by reducing either the number of low-frequency measurements or the number of current injections. This can result in a loss of spectral and spatial resolution if measurement configurations are not suitably optimized to compensate for the lost number of measurements.

## 6 Conclusions

The goal of this study was to investigate and establish spectral (i.e., multifrequency) EIT as a non-invasive tool for the characterization and monitoring of crop root systems. Based on working hypotheses derived from the state of science in the involved fields, including geophysics and plant science, we designed and conducted a controlled experiment in which the root systems of oilseed plants were monitored in a 2-D, water-filled rhizotron container. Since water does not exhibit a significant polarization response in the considered frequency range, the observed electrical polarization response could be attributed to the root systems.

The spectral EIT imaging results revealed a low-frequency polarization response of the root system, which enabled the successful delineation of the spatial extension of the root system. Based on a pixel-based Debye decomposition analysis of the spectral imaging results, we found a mean relaxation time of the root system's polarization signature in the covered frequency range of the order of 10 ms, corresponding to a frequency of the order of 15 Hz. Importantly, upon ongoing nutrient deprivation (with possibly anaerobic conditions), the magnitude of the overall polarization response steadily decreased and the spectral characteristics systematically changed, indicating changes in the length scales on which the polarization processes took place in the root system. The spectral EIT imaging results could be explained by the macroscopically observed and expected physiological response of the plant to the imposed stress situation. The identification of the root structures and processes controlling the root electrical signatures, however, was beyond the scope of this study given the inherent spatial resolution limits of

EIT. Nonetheless the recovered electrical signatures could be used in the future to develop and calibrate improved macroscopic root electrical models which incorporate microscopic processes.

We showed, for the first time (to the best of our knowledge), that spectral EIT is a capable, non-invasive method to image root system extension as well as to monitor changes associated with root physiological processes. Given the applicability of the method at both the laboratory and field scale, our results suggest an enormous potential of spectral EIT for the structural and functional imaging of root systems for various applications. In particular, at the field scale, non-invasive methods for root system characterization and imaging are lacking and EIT seems to be a very promising method to fill this gap. In future studies we will aim to further prove the suitability of spectral EIT to monitor physiological responses in different situations and to different stimuli, at both laboratory and field scales.

## 7 Data availability

Measured raw data, electrical imaging data, spectral analysis results, and Python scripts used to generate the figures can be accessed at doi:10.5281/zenodo.260087 (Weigand and Kemna, 2017).

**The Supplement related to this article is available online at doi:10.5194/bg-14-921-2017-supplement.**

*Competing interests.* The authors declare that they have no conflict of interest.

*Acknowledgements.* Parts of this work were funded by the Deutsche Forschungsgemeinschaft (DFG) in the framework of the project “Non-destructive characterization and monitoring of root structure and function at the rhizotron and field scale using spectral electrical impedance tomography” (KE 1138/1-1) and the collaborative research center “Patterns in soil-vegetation-atmosphere systems: monitoring, modeling and data assimilation” (SFB/TR 32). We are especially grateful to Egon Zimmermann and Matthias Kelter for valuable discussions regarding the measurement setup. We also thank Achim Walter, Johannes Pfeifer and Kerstin Nagel for technical support and discussions on root physiology in the initial phase of the work. The authors would also like to thank the three anonymous referees for their very constructive reviews, which lead to substantial improvements of the paper.

Edited by: P. Stoy

Reviewed by: three anonymous referees

## References

- al Hagrey, S.: Geophysical imaging of root-zone, trunk, and moisture heterogeneity, *J. Exp. Bot.*, 58, 839–854, doi:10.1093/jxb/erl237, 2007.
- al Hagrey, S. and Petersen, T.: Numerical and experimental mapping of small root zones using optimized surface and borehole resistivity tomography, *Geophysics*, 76, G25–G35, doi:10.1190/1.3545067, 2011.
- Alumbaugh, D. and Newman, G.: Image appraisal for 2-D and 3-D electromagnetic inversion, *Geophysics*, 65, 1455–1467, doi:10.1190/1.1444834, 2000.
- Amato, M., Bassi, B., Celano, G., Bitella, G., Morelli, G., and Rossi, R.: In situ detection of tree root distribution and biomass by multi-electrode resistivity imaging, *Tree Physiol.*, 28, 1441–1448, doi:10.1093/treephys/28.10.1441, 2008.
- Amato, M., Bitella, G., Rossi, R., Gómez, J. A., Lovelli, S., and Gomes, J. J. F.: Multi-electrode 3D resistivity imaging of alfalfa root zone, *Eur. J. Agron.*, 31, 213–222, doi:10.1016/j.eja.2009.08.005, 2009.
- Anderson, S. and Hopmans, J. (Eds.): *Soil-water-root Processes: Advances in Tomography and Imaging*, Soil Sci. Soc. Am., doi:10.2136/sssaspecpub61, 2013.
- Anderson, W. and Higinbotham, N.: Electrical resistances of corn root segments, *Plant Physiol.*, 57, 137–141, doi:10.1104/pp.57.2.137, 1976.
- Aubrecht, L., Staněk, Z., and Koller, J.: Electrical measurement of the absorption surfaces of tree roots by the earth impedance method: 1. Theory, *Tree Physiol.*, 26, 1105–1112, doi:10.1093/treephys/26.9.1105, 2006.
- Aulen, M. and Shipley, B.: Non-destructive estimation of root mass using electrical capacitance on ten herbaceous species, *Plant Soil*, 355, 41–49, doi:10.1007/s11104-011-1077-3, 2012.
- Barsoukov, E. and Macdonald, J. (Eds.): *Impedance spectroscopy: theory, experiment, and applications*, Wiley-Interscience, doi:10.1002/0471716243, 2005.
- Bayford, R.: Bioimpedance tomography (electrical impedance tomography), *Annual Reviews Biomedical Engineering*, 8, 63–91, doi:10.1146/annurev.bioeng.8.061505.095716, 2006.
- Beff, L., Günther, T., Vandoorne, B., Couvreur, V., and Javaux, M.: Three-dimensional monitoring of soil water content in a maize field using Electrical Resistivity Tomography, *Hydrol. Earth Syst. Sci.*, 17, 595–609, doi:10.5194/hess-17-595-2013, 2013.
- Benlloch-González, M., Fournier, J., and Benlloch, M.:  $K^+$  deprivation induces xylem water and  $K^+$  transport in sunflower: evidence for a co-ordinated control, *J. Exp. Bot.*, 61, 157–164, doi:10.1093/jxb/erp288, 2010.
- Binley, A. and Kemna, A.: DC resistivity and induced polarization methods, in: *Hydrogeophysics*, edited by: Rubin, Y. and Hubbard, S. S., Springer, the Netherlands, 129–156, doi:10.1007/1-4020-3102-5\_5, 2005.
- Binley, A., Slater, L., Fukes, M., and Cassiani, G.: Relationship between spectral induced polarization and hydraulic properties of saturated and unsaturated sandstone, *Water Resour. Res.*, 41, 1–13, doi:10.1029/2005WR004202, 2005.
- Boaga, J., Rossi, M., and Cassiani, G.: Monitoring soil-plant interactions in an apple orchard using 3D electrical resistivity tomography, *Procedia Environmental Sciences*, 19, 394–402, doi:10.1016/j.proenv.2013.06.045, 2013.
- Bücker, M. and Hördt, A.: Analytical modelling of membrane polarization with explicit parametrization of pore radii and the electrical double layer, *Geophys. J. Int.*, 194, 804–813, doi:10.1093/gji/ggt136, 2013.
- Cao, Y., Repo, T., Silvennoinen, R., Lehto, T., and Pelkonen, P.: An appraisal of the electrical resistance method for assessing root surface area, *J. Exp. Bot.*, 61, 2491–2497, doi:10.1093/jxb/erq078, 2010.
- Cao, Y., Repo, T., Silvennoinen, R., Lehto, T., and Pelkonen, P.: Analysis of the willow root system by electrical impedance spectroscopy, *J. Exp. Bot.*, 62, 351–358, doi:10.1093/jxb/erq276, 2011.
- Čermák, J., Ulrich, R., Staněk, Z., Koller, J., and Aubrecht, L.: Electrical measurement of tree root absorbing surfaces by the earth impedance method: 2. Verification based on allometric relationships and root severing experiments, *Tree Physiol.*, 26, 1113–1121, doi:10.1093/treephys/26.9.1113, 2006.
- Chloupek, O.: The relationship between electric capacitance and some other parameters of plant roots, *Biol. Plantarum*, 14, 227–230, doi:10.1007/BF02921255, 1972.
- Chloupek, O.: Die Bewertung des Wurzelsystems von Senfpflanzen auf Grund der dielektrischen Eigenschaften und mit Rücksicht auf den Endertrag, *Biol. Plantarum*, 18, 44–49, doi:10.1007/BF02922333, 1976.
- Claassen, N. and Barber, S.: A method for characterizing the relation between nutrient concentration and flux into roots of intact plants, *Plant Physiol.*, 54, 564–568, doi:10.1104/pp.54.4.564, 1974.
- Clarkson, D., Carvajal, M., Henzler, T., Waterhouse, R., Smyth, A., Cooke, D., and Steudle, E.: Root hydraulic conductance: diurnal aquaporin expression and the effects of nutrient stress, *J. Exp. Bot.*, 51, 61–70, doi:10.1093/jexbot/51.342.61, 2000.
- Cseresnyés, I., Tünde, T., Végh, K., Anton, A., and Rajkai, K.: Electrical impedance and capacitance method: A new approach for detection of functional aspects of arbuscular mycorrhizal colonization in maize, *European J. Soil Biol.*, 54, 25–31, doi:10.1016/j.ejsobi.2012.11.001, 2013.
- Daily, W., Ramirez, A., Binley, A., and LaBrecque, D.: Electrical resistance tomography – theory and practice, in: *Near-Surface Geophysics*, edited by: Butler, D., Vol. 154, chap. 17, Society of Exploration Geophysicists, Tulsa, OK, 525–550, doi:10.1190/1.9781560801719.ch17, 2005.
- Dalton, F.: In-situ root extent measurements by electrical capacitance methods, *Plant Soil*, 173, 157–165, doi:10.1007/BF00155527, 1995.
- Delhon, P., Gojon, A., Tillard, P., and Passama, L.: Diurnal regulation of  $NO_3^-$  uptake in soybean plants I. Changes in  $NO_3^-$  influx, efflux, and N utilization in the plant during the day/night cycle, *J. Exp. Bot.*, 46, 1585–1594, doi:10.1093/jxb/46.10.1585, 1995.
- Dietrich, R., Bengough, A., Jones, H., and White, P.: Can root electrical capacitance be used to predict root mass in soil?, *Ann. Bot.*, 112, 457–464, doi:10.1093/aob/mct044, 2013.
- Dukhin, S. S. and Shilov, V. N.: *Dielectric Phenomena and the Double Layer in Disperse Systems and Polyelectrolytes*, Wiley, New York, 1974.
- Dunbabin, V., Postma, J., Schnepp, A., Pagès, L., Javaux, M., Wu, L., Leitner, D., Chen, Y., Rengel, Z., and Diggle, A.: Modelling root-soil interactions using three-dimensional models of

- root growth, architecture and function, *Plant Soil*, 372, 93–124, doi:10.1007/s11104-013-1769-y, 2013.
- Dvořák, M., Černohorská, J., and Janáček, K.: Characteristics of current passage through plant tissue, *Biol. Plantarum*, 23, 306–310, doi:10.1007/BF02895374, 1981.
- Ellis, T., Murray, W., and Kavalieris, L.: Electrical capacitance of bean (*Vicia faba*) root systems was related to tissue density – a test for the Dalton Model, *Plant Soil*, 366, 575–584, doi:10.1007/s11104-012-1424-z, 2013.
- Fixman, M.: Charged Macromolecules in External Fields. 2. Preliminary Remarks on the Cylinder, *Macromolecules*, 13, 711–716, doi:10.1021/ma60075a043, 1980.
- Flores Orozco, A., Kemna, A., Oberdörster, C., Zschornack, L., Leven, C., Dietrich, P., and Weiss, H.: Delineation of subsurface hydrocarbon contamination at a former hydrogenation plant using spectral induced polarization imaging, *J. Contam. Hydrol.*, 136, 131–144, doi:10.1016/j.jconhyd.2012.06.001, 2012a.
- Flores Orozco, A., Kemna, A., and Zimmermann, E.: Data error quantification in spectral induced polarization imaging, *Geophysics*, 77, E227–E237, doi:10.1190/geo2010-0194.1, 2012b.
- Flores Orozco, A., Williams, K., and Kemna, A.: Time-lapse spectral induced polarization imaging of stimulated uranium bioremediation, *Near Surf. Geophys.*, 11, 531–544, doi:10.3997/1873-0604.2013020, 2013.
- Friedel, S.: Resolution, stability and efficiency of resistivity tomography estimated from a generalized inverse approach, *Geophys. J. Int.*, 153, 305–316, doi:10.1046/j.1365-246X.2003.01890.x, 2003.
- Gregory, P., Hutchison, D., Read, D., Jenneson, P., Gilboy, W., and Morton, E.: Non-invasive imaging of roots with high resolution X-ray micro-tomography, in: Roots: The Dynamic Interface between Plants and the Earth, Springer, 351–359, doi:10.1023/A:1026179919689, 2003.
- Günther, T. and Martin, T.: Spectral two-dimensional inversion of frequency-domain induced polarization data from a mining slag heap, *J. Appl. Geophys.*, 135, 436–448, doi:10.1016/j.jappgeo.2016.01.008, 2016.
- Heege, H.: Precision in Crop Farming: Site Specific Concepts and Sensing Methods: Applications and Results, Springer Science & Business Media, Springer, the Netherlands, 2013.
- Heršmanská, A., Středa, T., and Chloupek, O.: Improved wheat grain yield by a new method of root selection, *Agron. Sustain. Dev.*, 35, 195–202, doi:10.1007/s13593-014-0227-4, 2015.
- Hose, E., Clarkson, D., Steudle, E., Schreiber, L., and Hartung, W.: The exodermis: a variable apoplastic barrier, *J. Exp. Bot.*, 52, 2245–2264, doi:10.1093/jexbot/52.365.2245, 2001.
- Huisman, J., Zimmermann, E., Esser, O., Haegel, F., Treichel, A., and Vereecken, H.: Evaluation of a novel correction procedure to remove electrode impedance effects from broadband SIP measurements, *J. Appl. Geophys.*, 135, 466–473, doi:10.1016/j.jappgeo.2015.11.008, 2015.
- Javaux, M., Couvreur, V., Vanderborght, J., and Vereecken, H.: Root water uptake: From three-dimensional biophysical processes to macroscopic modeling approaches, *Vadose Zone J.*, 12, 1–16, doi:10.2136/vzj2013.02.0042, 2013.
- Johnson, T., Slater, L., Ntarlagiannis, D., Day-Lewis, F., and Elwaseif, M.: Monitoring groundwater-surface water interaction using time-series and time-frequency analysis of transient three-dimensional electrical resistivity changes, *Water Resour. Res.*, 48, W07506, doi:10.1029/2012WR011893, 2012.
- Kelter, M., Huisman, J., Zimmermann, E., Kemna, A., and Vereecken, H.: Quantitative imaging of spectral electrical properties of variably saturated soil columns, *J. Appl. Geophys.*, 123, 333–344, doi:10.1016/j.jappgeo.2015.09.001, 2015.
- Kemna, A.: Tomographic inversion of complex resistivity – theory and application, PhD thesis, Ruhr-Universität Bochum, doi:10.1111/1365-2478.12013, 2000.
- Kemna, A., Binley, A., Cassiani, G., Niederleithinger, E., Revil, A., Slater, L., Williams, K., Flores Orozco, A., Haegel, F., Hoerdt, A., Kruschwitz, S., Leroux, V., Titov, K., and Zimmermann, E.: An overview of the spectral induced polarization method for near-surface applications, *Near Surf. Geophys.*, 10, 453–468, doi:10.3997/1873-0604.2012027, 2012.
- Kemna, A., Huisman, J., Zimmermann, E., Martin, R., Zhao, Y., Treichel, A., Flores Orozco, A., and Fechner, T.: Broadband electrical impedance tomography for subsurface characterization using improved corrections of electromagnetic coupling and spectral regularization, in: Tomography of the Earth's Crust: From Geophysical Sounding to Real-Time Monitoring, Springer, 1–20, doi:10.1007/978-3-319-04205-3\_1, 2014.
- Kinraide, T.: Use of a Gouy-Chapman-Stern model for membrane-surface electrical potential to interpret some features of mineral rhizotoxicity, *Plant Physiol.*, 106, 1583–1592, 1994.
- Kinraide, T. and Wang, P.: The surface charge density of plant cell membranes ( $\sigma$ ): an attempt to resolve conflicting values for intrinsic  $\sigma$ , *J. Exp. Bot.*, 61, 2507–2518, doi:10.1093/jxb/erq082, 2010.
- Kinraide, T., Yermiyahu, U., and Rytwo, G.: Computation of surface electrical potentials of plant cell membranes correspondence to published zeta potentials from diverse plant sources, *Plant Physiol.*, 118, 505–512, doi:10.1104/pp.118.2.505, 1998.
- Kormanek, M., Głab, T., and Klimek-Kopyra, A.: Modification of the tree root electrical capacitance method under laboratory conditions, *Tree Physiol.*, 36, 121–127, doi:10.1093/treephys/tpv088, 2015.
- Kruschwitz, S., Binley, A., Lesmes, D., and Elshenawy, A.: Textural controls on low-frequency electrical spectra of porous media, *Geophysics*, 75, WA113, doi:10.1190/1.3479835, 2010.
- Kyle, A., Chan, C., and Minchinton, A.: Characterization of three-dimensional tissue cultures using electrical impedance spectroscopy, *Biophys. J.*, 76, 2640–2648, doi:10.1016/S0006-3495(99)77416-3, 1999.
- LaBrecque, D. and Ward, S.: Two-dimensional cross-borehole resistivity model fitting, *Geotechnical and Environmental Geophysics*, 1, 51–57, 1990.
- LaBrecque, D., Ramirez, A., Daily, W., Binley, A., and Schima, S.: ERT monitoring of environmental remediation processes, *Meas. Sci. Technol.*, 7, 375–383, doi:10.1088/0957-0233/7/3/019, 1996.
- Leroy, P., Revil, A., Kemna, A., Cosenza, P., and Ghorbani, A.: Complex conductivity of water-saturated packs of glass beads, *J. Colloid Interf. Sci.*, 321, 103–117, doi:10.1016/j.jcis.2007.12.031, 2008.
- Lesmes, D. and Frye, K.: Influence of pore fluid chemistry on the complex conductivity and induced polarization responses of Berea sandstone, *J. Geophys. Res.*, 106, 4079–4090, doi:10.1029/2000JB900392, 2001.

- Li, Z., Liu, Y., Zheng, Y., and Xu, R.: Zeta potential at the root surfaces of rice characterized by streaming potential measurements, *Plant Soil*, 386, 237–250, doi:10.1007/s11104-014-2259-6, 2015.
- Loke, M., Chambers, J., Rucker, D., Kuras, O., and Wilkinson, P.: Recent developments in the direct-current geoelectrical imaging method, *J. Appl. Geophys.*, 95, 135–156, doi:10.1016/j.jappgeo.2013.02.017, 2013.
- Lyklema, J.: Fundamentals of interface and colloid science: solid-liquid interfaces, Vol. 2, Academic press, London, UK, 2005.
- Lyklema, J., Dukhin, S., and Shilov, V.: The relaxation of the double layer around colloidal particles and the low-frequency dielectric dispersion: Part I. Theoretical considerations, *Journal of Electroanalytical Chemistry and Interfacial Electrochemistry*, 143, 1–21, doi:10.1016/S0022-0728(83)80251-4, 1983.
- Mancuso, S.: Measuring roots: an updated approach, Springer Science & Business Media, doi:10.1007/978-3-642-22067-8, Springer, Heidelberg, Dordrecht, London, New York, 2012.
- Martin, T. and Günther, T.: Complex resistivity tomography (CRT) for fungus detection on standing oak trees, *Eur. J. Forest Res.*, 132, 765–776, doi:10.1007/s10342-013-0711-4, 2013.
- Martínez-Ballesta, M., Rodríguez-Hernández, M., Alcaraz-López, C., Mota-Cadenas, C., Muriles, B., and Carvajal, M.: Plant hydraulic conductivity: The aquaporins contribution, Hydraulic conductivity – issues, determination and applications, Rijeka: In Tech, 103–21, doi:10.5772/18580, 2011.
- Metzner, R., Eggert, A., van Dusschoten, D., Pflugfelder, D., Gerth, S., Schurr, U., Uhlmann, N., and Jahnke, S.: Direct comparison of MRI and X-ray CT technologies for 3D imaging of root systems in soil: potential and challenges for root trait quantification, *Plant Meth.*, 11, 17, doi:10.1186/s13007-015-0060-z, 2015.
- Nordsiek, S. and Weller, A.: A new approach to fitting induced-polarization spectra, *Geophysics*, 73, F235–F245, doi:10.1190/1.2987412, 2008.
- Ozier-Lafontaine, H. and Bajazet, T.: Analysis of root growth by impedance spectroscopy (EIS), *Plant Soil*, 277, 299–313, doi:10.1007/s11104-005-7531-3, 2005.
- Pelton, W., Ward, S., Hallof, P., Sill, W., and Nelson, P.: Mineral discrimination and removal of inductive coupling with multi-frequency IP, *Geophysics*, 43, 588–609, doi:10.1190/1.1440839, 1978.
- Pierret, A., Doussan, C., Garrigues, E., and Mc Kirby, J.: Observing plant roots in their environment: current imaging options and specific contribution of two-dimensional approaches, *Agronomie*, 23, 471–479, doi:10.1051/agro:2003019, 2003.
- Prodan, C. and Prodan, E.: The dielectric behaviour of living cell suspensions, *J. Phys. D*, 32, 335–343, 1999.
- Prodan, E., Prodan, C., and Miller Jr., J.: The dielectric response of spherical live cells in suspension: an analytic solution, *Biophys. J.*, 95, 4174–4182, doi:10.1529/biophysj.108.137042, 2008.
- Razilov, I. and Dukhin, S.: Simultaneous influence of concentration polarization of the diffuse layer and polarization of the Stern layer according to the mechanism of bound counterions at arbitrary magnitudes of the relaxation parameter, *Colloid J. Russ. Acad.*, 57, 364–371, 1995.
- Repo, T., Cao, Y., Silvennoinen, R., and Ozier-Lafontaine, H.: Electrical impedance spectroscopy and roots, in: *Measuring Roots*, edited by: Mancuso, S., Springer, 25–49, doi:10.1007/978-3-642-22067-8\_2, 2012.
- Repo, T., Korhonen, A., Laukkanen, M., Lehto, T., and Silvennoinen, R.: Detecting mycorrhizal colonisation in Scots pine roots using electrical impedance spectra, *Biosyst. Eng.*, 121, 139–149, doi:10.1016/j.biosystemseng.2014.02.014, 2014.
- Revil, A. and Florsch, N.: Determination of permeability from spectral induced polarization in granular media, *Geophys. J. Int.*, 181, 1480–1498, doi:10.1111/j.1365-246X.2010.04573.x, 2010.
- Revil, A., Karaoulis, M., Johnson, T., and Kemna, A.: Review: Some low-frequency electrical methods for subsurface characterization and monitoring in hydrogeology, *Hydrogeol. J.*, 20, 617–658, doi:10.1007/s10040-011-0819-x, 2012.
- Revil, A., Florsch, N., and Camerlynck, C.: Spectral induced polarization porosimetry, *Geophys. J. Int.*, 198, 1016–1033, doi:10.1093/gji/ggu180, 2014.
- Rossi, R., Amato, M., Bitella, G., Bochicchio, R., Ferreira Gomes, J., Lovelli, S., Martorella, E., and Favale, P.: Electrical resistivity tomography as a non-destructive method for mapping root biomass in an orchard, *Eur. J. Soil Sci.*, 62, 206–215, doi:10.1111/j.1365-2389.2010.01329.x, 2011.
- Schraut, D., Heilmeier, H., and Hartung, W.: Radial transport of water and abscisic acid (ABA) in roots of Zea mays under conditions of nutrient deficiency, *J. Exp. Bot.*, 56, 879–886, doi:10.1093/jxb/eri080, 2005.
- Schwan, H.: Electrical Properties of Tissue and Cell Suspensions, Vol. 5 of *Advances in Biological and Medical Physics*, Elsevier, 147–209, doi:10.1016/B978-1-4832-3111-2.50008-0, 1957.
- Schwarz, G.: A theory of the low-frequency dielectric dispersion of colloidal particles in electrolyte solution, *J. Phys. Chem.*, 66, 2636–2642, doi:10.1021/j100818a067, 1962.
- Singha, K., Day-Lewis, F., Johnson, T., and Slater, L.: Advances in interpretation of subsurface processes with time-lapse electrical imaging, *Hydrol. Process.*, 29, 1549–1576, doi:10.1002/hyp.10280, 2014.
- Shayedin, I. and Doussan, C.: Estimation of the spatial variability of root water uptake of maize and sorghum at the field scale by electrical resistivity tomography, *Plant Soil*, 319, 185–207, doi:10.1007/s11104-008-9860-5, 2009.
- Tarasov, A. and Titov, K.: On the use of the Cole-Cole equations in spectral induced polarization, *Geophys. J. Int.*, 195, 352–356, doi:10.1093/gji/ggt251, 2013.
- Tinker, P. and Nye, P.: Solute movement in the rhizosphere, Oxford University Press, Inc., New York, doi:10.1046/j.1365-2389.2001.00418-2.x, 2000.
- Titov, K., Komarov, V., Tarasov, V., and Levitski, A.: Theoretical and experimental study of time domain-induced polarization in water-saturated sands, *J. Appl. Geophys.*, 50, 417–433, doi:10.1016/S0926-9851(02)00168-4, 2002.
- Uhlmann, D. and Hakim, R.: Derivation of distribution functions from relaxation data, *J. Phys. Chem. Solids*, 32, 2652–2655, doi:10.1016/S0022-3697(71)80114-2, 1971.
- Urban, J., Bequet, R., and Mainiero, R.: Assessing the applicability of the earth impedance method for in situ studies of tree root systems, *J. Exp. Bot.*, 62, 1857–1869, doi:10.1093/jxb/erq370, 2011.
- Walker, J.: Electrical AC resistance and capacitance of Zea mays L., *Plant Soil*, 23, 270–274, doi:10.1007/BF01358354, 1965.
- Wang, P., Zhou, D.-M., Li, L.-Z., and Li, D.-D.: What role does cell membrane surface potential play in ion-plant interactions,

- Plant Signaling & Behavior, 4, 42–43, doi:10.4161/psb.4.1.7270, 2009.
- Wang, P., Kinraide, T., Zhou, D., K., P. M., and Peijnenburg, W.: Plasma membrane surface potential: dual effects upon ion uptake and toxicity, *Plant Physiol.*, 155, 808–820, doi:10.1104/pp.110.165985, 2011.
- Wang, Y.-M., Kinraide, T., Wang, P., Zhou, D., and Hao, X.: Modeling rhizotoxicity and uptake of Zn and Co singly and in binary mixture in wheat in terms of the cell membrane surface electrical potential, *Environ. Sci. Technol.*, 47, 2831–2838, doi:10.1021/es3022107, 2013.
- Weigand, M. and Kemna, A.: Debye decomposition of time-lapse spectral induced polarisation data, *Comput. Geosci.*, 86, 34–45, doi:10.1016/j.cageo.2015.09.021, 2016.
- Weigand, M. and Kemna, A.: Data and results for manuscript “Multi-frequency electrical impedance tomography as a non-invasive tool to characterize and monitor crop root systems”, Data set, Zenodo, doi:10.5281/zenodo.260087, 2017.
- Whalley, W., Binley, A., Watts, C., Shanahan, P., Dodd, I., Ober, E., Ashton, R., Webster, C., White, R., and Hawkesford, M. J.: Methods to estimate changes in soil water for phenotyping root activity in the field, *Plant Soil*, 1–16, doi:10.1007/s11104-016-3161-1, 2017.
- Willatt, S., Struss, R., and Taylor, H.: In situ root studies using neutron radiography, *Agron. J.*, 70, 581–586, doi:10.2134/agronj1978.00021962007000040016x, 1978.
- Zanetti, C., Weller, A., Vennetier, M., and Mériaux, P.: Detection of buried tree root samples by using geoelectrical measurements: a laboratory experiment, *Plant Soil*, 339, 273–283, doi:10.1007/s11104-010-0574-0, 2011.
- Zhao, Y., Zimmerman, E., Huisman, J., Treichel, A., Wolters, B., van Waasen, S., and Kemna, A.: Broadband EIT borehole measurements with high phase accuracy using numerical corrections of electromagnetic coupling effects, *Meas. Sci. Technol.*, 24, 085005, doi:10.1088/0957-0233/24/8/085005, 2013.
- Zimmermann, E., Kemna, A., Berwix, J., Glaas, W., and Vereecken, H.: EIT measurement system with high phase accuracy for the imaging of spectral induced polarization properties of soils and sediments, *Meas. Sci. Technol.*, 19, 094010, doi:10.1088/0957-0233/19/9/094010, 2008.